Frontiers + Innovation
2009 CSPG CSEG CWLS CONVENTION • CALGARY, ALBERTA, CANADA

Salt Mapping Using 3D-marine CSEM Surveys

J.J. Zach (jjz@emgs.com), M.A. Frenkel (mfrenkel@emgs.com),
A.M. Ostvedt-Ghazi (amghazi@emgs.com), S. Goldstein (sg@emgs.com),
A. Kumar (akumar@emgs.com), T. Pham (pham@emgs.com)
EMGS Americas, 16000 Barkers Point Lane, Houston TX, 77079

Summary

Since the inception of marine CSEM methods for hydrocarbon exploration, or Seabed Logging, in 2002, great advances in hardware and operations have laid the groundwork to enable grid acquisitions for 3D imaging of the resistivity distribution in the subsurface. These are fast becoming a standard part of the repertoire of geophysical probes for prospect ranking, evaluation and frontier exploration.

One of the major challenges in the Gulf of Mexico (GoM) and other exploration areas for both seismic and electromagnetic surveys is the fact that salt is frequently found at all burial depths. Mapping these salt structures is therefore of paramount importance, and marine CSEM methods can both provide an alternative to seismic top-salt mapping in frontier exploration, and a valuable complementary measurement in cases where high-resolution seismic data have already been acquired. The objective of the present study is to map the top-salt distribution in an area of the GoM which exhibits complex salt structures, and in which a recent CSEM exploration survey with 3D grid acquisition has been conducted. The data set is inverted using a 3D inversion scheme with Hessian-based optimization and a fast finite-difference time-domain forward solver, and results are compared with existing 3D seismic data and well control.

Introduction

Marine CSEM surveys have experienced a renaissance in this decade after first being applied for hydrocarbon detection (e.g., Eidesmo et al., 2002). Continued evolution in operational accuracy and hardware sensitivity have resulted in a vast improvement in data quality, which enable full 3D inversion, including wide-azimuth data, of complex receiver grids on the seafloor. Thus, 3D imaging of complex geology using marine CSEM, either as a standalone method or in conjunction with other geophysical probes, is increasingly adopted by exploration and production companies. Recent case studies targeting hydrocarbons include Carrazone et al. (2008), Price et al. (2008) and Plessix, van der Sman (2008).

To date, most solutions brought forward to solve the 3D marine CSEM problem rely on an iterative approach with repeated computation of the gradient of a misfit functional with respect to the discrete conductivity grid: $g = \partial\varepsilon/\partial\sigma$, where the L2-norm is the most common choice for the data misfit $\varepsilon = \sum_{s,r,\omega,F} (\mathrm{Weight})(\vec{x}_r \mid \vec{x}_s ; \omega)\left|\Delta F_i(\vec{x}_r \mid \vec{x}_s ; \omega)\right|^2$. Differences lie mainly in the forward operators, the gridding of the forward and/or inversion grid and preconditioning approaches used in the optimization steps. The 3D case study presented here was inverted following Zach et al., 2008, using a quasi-Newton method, where the inverse Hessian is approximated by an outer product formulation of the vectors of an integer number of past iterations' update steps and gradient changes. The forward problem is solved with a finite-difference time-domain solver, and the gradient is calculated at each iteration using a Green's function approach, based on the assumption of the first Born-approximation applied to the difference field between synthetic and real data. For details, as well as other references, see Zach et al. (2008a). Notable among the most recent contributions on inversion methodology are Commer and Newman (2008) on joint CSEM and MT inversion, as well as Jing et al. (2008), which shows the importance of anisotropy in many surveys.

While seismic methods are effective in mapping top-salt horizons, structural and electromagnetic geological boundaries do not need to coincide, so that the acquisition of both CSEM and seismic surveys greatly enhance the value of both (e.g., Norman et al. 2008). Magnetotelluric and potential methods, which are valuable in mapping the bulk volume of buried salt bodies (Wu et al., 2008), do not usually have sufficient resolution to accurately resolve the top salt horizon.

Methodology

Data from the 3D grid shown in figure 1 (left) was conditioned for 3D inversion, producing frequency-domain data and noise estimates using the methodology described in Zach et al. (2008b). The time-domain pulse was designed to have the transmitted energy concentrated on the four main frequency modes 0.25, 0.5, 0.75 and 1.0Hz. While towing the source over each receiver was still necessary to accurately determine its orientation, azimuthal data could be recovered which is accurate to within 5% in magnitude and 5 degrees in phase.

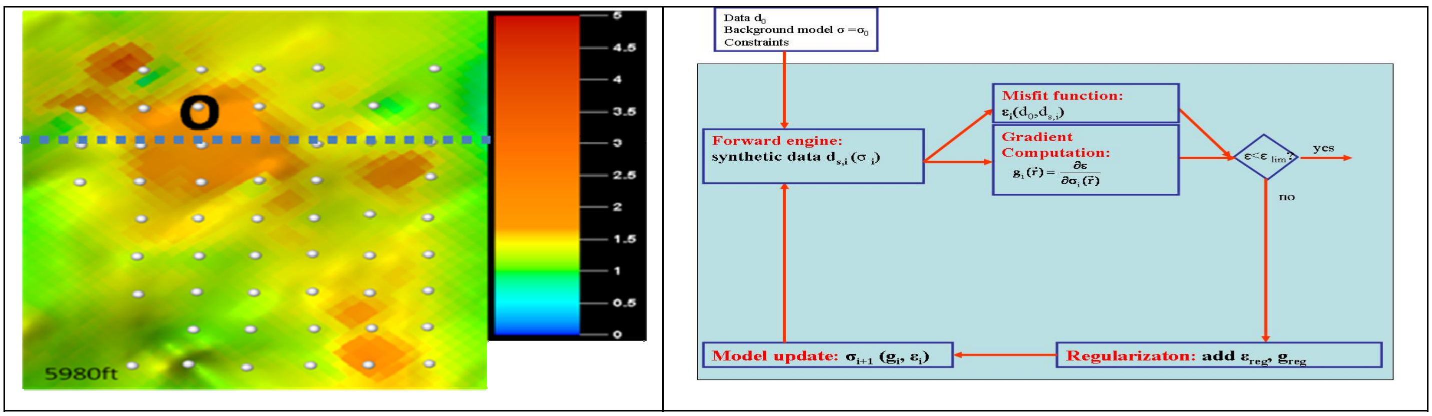

Figure 1: Left: 3D grid of receiver locations (representative, and specifically used here) for 3D inversion with 900m receiver spacing; shown is the resistivity map from full 3D inversion at a certain reservoir depth slice; the top salt horizon which is the subject of this study is located at greater depths. Right: iterative loop for Hessian-based 3D inversion (from Zach et al., 2008).

Plane-layer inversions of half the receivers were run as a pre-stage to the full gradient-based 3D inversion, to identify general trends and to determine an appropriate starting model. 3D inversion is more sensitive to large-scale geologic trends not being taken into account in the starting model, in particular in the shallow subsurface. The plane-layer global inversion scheme (Roth and Zach, 2007), based on simulated annealing, is used to invert individual receiver data for 2-3 frequencies and for the Ex- and Hy-fields simultaneously. The depth is discretized using a stretched grid with 43 bins from mudline, and a smoothness constraint of 1Ωm/bin renders the result independent of any a priori guesses. Using an exponential cooling scheme, convergence is typically reached after 10^4 plane layer forward steps.

The inversion proceeds in the iterative loop shown in figure 1 (right), where the input consists of the starting model and the conditioned data including weights. Using the estimated noise at each frequency mode, a binary weighting scheme is employed with a SNR-cutoff of 24 dB. In an exploration scenario typically given for salt mapping, no regularization other than conductivity bounds between salt water (3S/m) and 0.01S/m are assumed. The latter is the lowest conductivity which can be practically obtained in an unconstrained imaging scheme given frequencies of ~0.1-1 Hz. To improve convergence, the depth weighting preconditioners and optimization of the logarithm of the conductivity are used. The preconditioners, along with a gradient muting approach to minimize acquisition imprints, are described in Zach et al. (2008a).

Case study

Figure 2 shows results from a plane-layer inversion, in which data match to within the measurement accuracy was achieved after 10000 simulated-annealing cooling steps. For shorter offsets, where the plane layer inversion result is more reliable, resistivities between 1.5-3 Ωm are observed, where the fine structure is associated with layers of relatively resistive shale. Beyond 600-800 m below mudline, a conductive layer is recovered, which is associated with brine-saturated sandstone. At depths greater than 1.3-2 km below mudline, the resistivity gradually increases, signifying the appearance of salt. The basic features are qualitatively repeated for all receivers, however, for the detailed top-salt mapping using 3D inversion, the only plane layer- result we use is the average resistivity of the first 500m below mudline, which is about 2 Ωm.

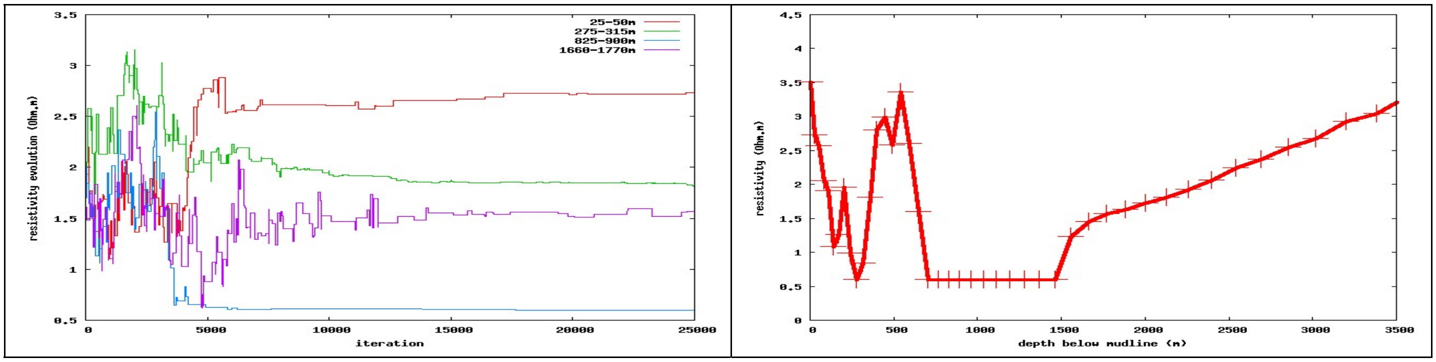

Figure 2: Plane-layer inversion of the receiver indicated as a black cross in figure 1, using a simulated annealing-approach. Left: evolution of selected depth-bins during cooling; Right: resulting resistivity-depth profile.

The qualitative predictions from plane-layer inversion are confirmed in the 3D-inversion result, a projection from which onto one grid line is shown in figure 3. The result was achieved by inverting the electric field only for the four main frequencies. The top-salt horizon from seismic interpretation is recovered to within 50-150 m, where the divergence could be due to a conductive halo of dissolved salt causing an increased salt resistivity deeper within the salt body as imaged by 3D seismic. Convergence to within the measurement accuracy is reached within 150 iterations, where a sample of the initial versus final data mismatch is shown in figure 4, along with the evolution of the misfit functional.

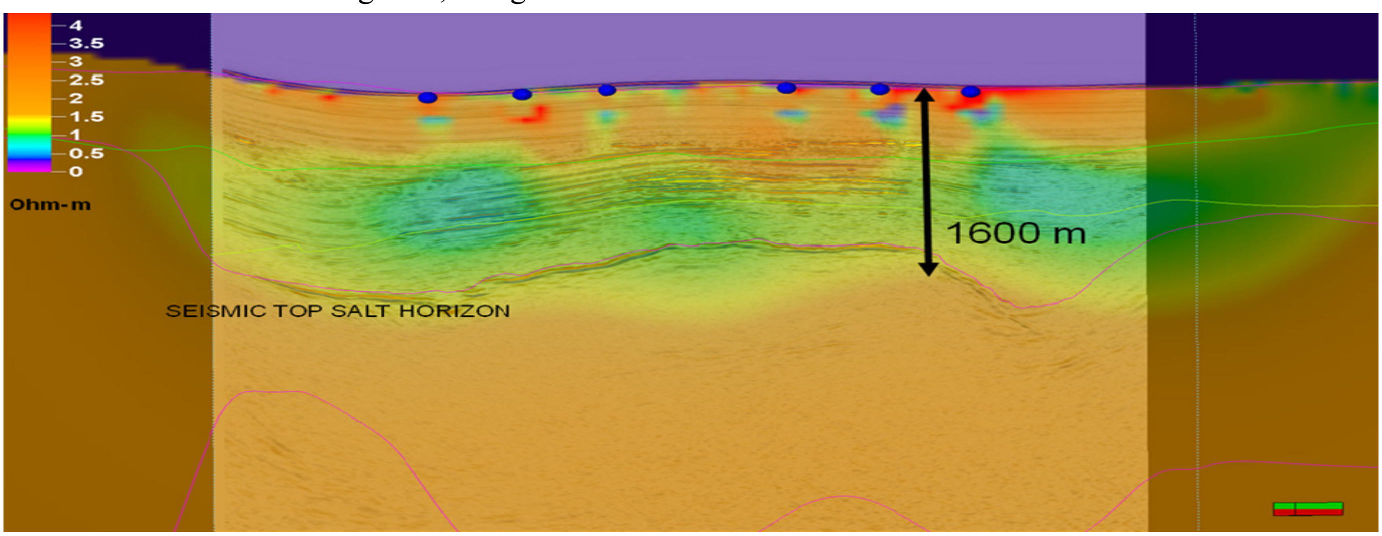

Figure 3: Projection of the resistivity cube from the final 3D inversion after result onto the line marked blue on figure 1, overlaid with a 3D seimics-image, along with the interpreted seismic top-salt horizon. The top-salt horizon is recovered to within 50-150 m, whereas the conductive salt boundary could differ from the mechanical boundary. Features in the subsurface known from well control and extensive seismic data, including the brine-saturated sandstone and the shale in shallow regions, are also recovered.

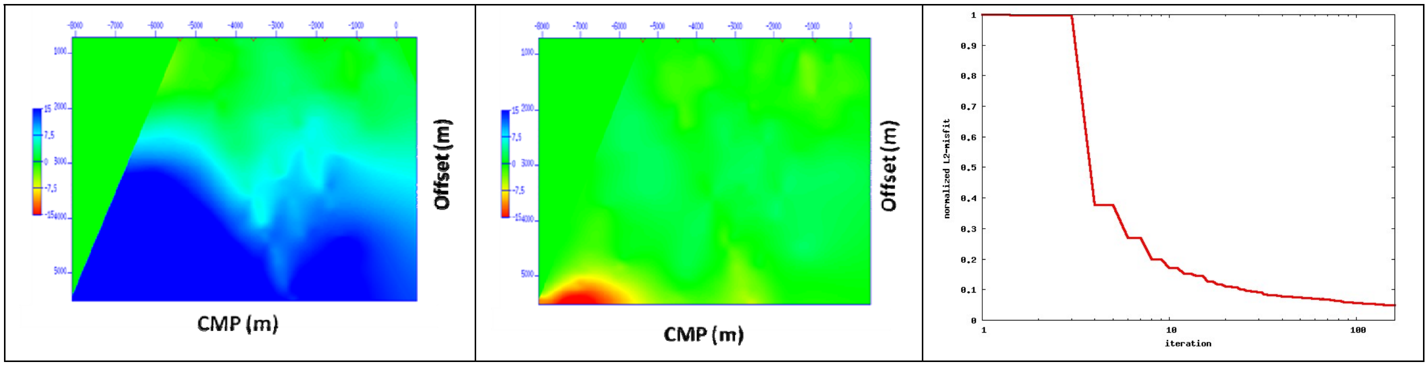

Figure 4: Left (center) panel: data misfit for initial (final) model in the phase for the f=0.5 Hz-mode, showing convergence to within the measurement accuracy (representative for magnitude and phase for all frequencies). Right panel: evolution of the misfit functional versus iteration number.

While real salt resistivities in the GoM have been observed to be at least several tens of Ωm, which is due to smearing-out effects caused by the CSEM sensitivity proportional to the target transverse resistance (Δρ)(Δz). However, to within existing well control, regions above the salt have been quantitatively confirmed.

Conclusions

The use of marine CSEM methods to map complex top salt structures in 3D is demonstrated with characteristic vertical accuracy (≤10% of burial depth). This implies the basic applicability of the marine CSEM/SBL method to typical "salt provinces" such as the GoM, which we intend to show in the future.

Acknowledgements

We thank the geoscientists of our E&P industry partner, which wished to remain confidential, for many valuable discussions as well as their agreement to show these data. We further would like to thank EMGS ASA for supporting this study and permitting its publication.

References

Carrazone, J.J., Dickens, T.A., Green, K.E., Jing, C., Wahrmund, L.A., Willen, D.E., Commer, M., Newman, G.A. (2008) Inversion study of a large marine CSEM survey. *SEG 2008 Expanded Abstracts*, Las Vegas, NV, USA.

Commer, M., Newman, G.A. (2008) Optimal conductivity reconstruction using three-dimensional joint and model-based inversion for controlled-source and magnetotelluric data, *SEG 2008 Expanded Abstracts*, Las Vegas, NV, USA.

Eidesmo, T., Ellingsrud, S., MacGregor, L.M., Constable, S., Sinha, M.C., Johansen, S., Kong, F.N. and Westerdahl, H. (2002) Sea Bed Logging (SBL), a new method for remote and direct identification of hydrocarbon filled layers in deepwater areas. *First Break*, 20, 144-152.

Jing, C., Green, K.E., Willen, D.E. (2008) CSEM inversion: Impact of anisotropy, data coverage, and initial models. *SEG 2008 Expanded Abstracts*, Las Vegas, NV, USA.

Norman, T., Christensen, O., Zach, J.J., Eiken, O., Tjåland, E. (2008) Planning Time-lapse CSEM-surveys for Joint Seismic-EM Monitoring of Geological Carbon Dioxide Injection. *EAGE Budapest 2008* CO2 Geological Storage Workshop.

Plessix, R.-E., van der Sman, P. (2008) Regularized and blocky controlled source electromagnetic inversion. *PIERS 2008*, Cambridge, Mass.

Price, A., Turpin, P., Erbetta, M., Watts, D., Cairns, G. (2008) 1D, 2D and 3D modeling and inversion of 3D CSEM data offshore West Africa. *SEG 2008 Expanded Abstracts*, Las Vegas, NV, USA.

Roth, F., Zach, J.J. (2007) Inversion of marine CSEM data using up-down wavefield separation and simulated annealing. *SEG 2007 Expanded Abstracts*, San Antonio, TX, USA.

Wu, X., Sandberg, S., Roper, T. (2008) Three-dimensional marine magnetotelluric resolution for subsalt imaging and case study in the gulf of Mexico, *SEG 2008 Expanded Abstracts*, Las Vegas, NV, USA.

Zach, J.J., Bjørke, A.K., Støren, T., Maaø, F. (2008a) 3D inversion of marine CSEM data using a fast finite-difference time-domain forward code and approximate Hessian-based optimization. *SEG 2008 Expanded Abstracts*, Las Vegas, NV, USA.

Zach, J.J., Roth, F., Yuan, H. (2008b) Data preprocessing and starting model preparation for 3D inversion of marine CSEM surveys. *EAGE 2008 Expanded Abstracts*, Rome, Italy.